Fission of ^{240}Pu with Symmetry-Restored Density Functional Theory

P. Marević and N. Schunck

Nuclear and Chemical Sciences Division, Lawrence Livermore National Laboratory, Livermore, California 94551, USA

Nuclear fission plays an important role in fundamental and applied science, from astrophysics to nuclear engineering, yet it remains a major challenge to nuclear theory. Theoretical methods used so far to compute fission observables rely on symmetry-breaking schemes where basic information on the number of particles, angular momentum, and parity of the fissioning nucleus is lost. In this Letter, we analyze the impact of restoring broken symmetries in the benchmark case of ^{240}Pu.

Introduction.—Nuclear fission, the process of splitting an atomic nucleus into two or more fragments, is a key ingredient for modeling nucleosynthesis, as it prevents the production of superheavy elements and its products (fission fragments, neutrons, and photons) impact the astrophysical reaction rates [1–5]. Detailed knowledge of the fission channels (spontaneous, neutron-induced, etc.) of selected actinide nuclei is also at the heart of important societal applications in medicine, energy production, nuclear forensics and safeguards, etc. [6]. In spite of recent advances in experimental techniques [7,8], measurements are not always possible and theoretical simulations that model the entire process leading to the formation and decay of fission fragments are mandatory.

Despite formidable efforts over the past eighty years, a fully microscopic description of the fission phenomenon based on nuclear forces among protons and neutrons and quantum many-body methods remains a challenge [9,10]. Nuclear density functional theory (DFT) is currently the only fully quantum-mechanical framework that can be used to compute fission observables, such as spontaneous fission half-lives [11] or fission fragment distributions [12–18]. Time-dependent DFT provides a natural framework to explain the energy sharing among the fragments [19–21], which is key to predicting their deexcitation.

Following the initial insight of Bohr and Wheeler, most DFT-based approaches to fission are built upon the assumption that a small set of collective degrees of freedom (typically related to the deformation of the nuclear shape) drives the fission process [10,22,23]. This description is formalized through the concept of spontaneous symmetry breaking: the intrinsic nuclear density does not conserve symmetries of the nuclear Hamiltonian [24,25]. In particular, the geometrical deformation of a nucleus is manifested by the breaking of rotational, axial, or reflection symmetry; nuclear superfluidity [26] by the breaking of particle number symmetry, etc. The corresponding potential energy surfaces (PESs) encode the total energy as a function of order parameters associated with breaking each symmetry.

They can be used to infer important quantities of interest, from tunneling probabilities for spontaneous fission half-lives [11], to the determination of initial states for time-dependent approaches [20,21], or basis states for quantum configuration mixing with the generator coordinate method (GCM) [27,28]. The most advanced PESs for fission studies are based on solving the Hartree-Fock-Bogoliubov (HFB) equation with Skyrme [29,30], Gogny [31,32], or relativistic [33,34] functionals.

However, such approaches conceal the basic information on quantum numbers related to each broken symmetry, such as the particle number, angular momentum, and parity of a nucleus. Restoring these symmetries is especially important to model different fission channels. For example, symmetry-breaking theory is incapable of distinguishing between the neutron-induced fission of ^{235}U and the photofission of ^{236}U [35]. In both cases, the compound nucleus is the same, ^{236}U, but the spin-parity distribution can be substantially different since ^{235}U(n, f) involves coupling the ^{235}U ground-state angular momentum $J = 7/2$ with the spin distribution of the neutron beam, while ^{236}U(γ, f) couples the spin 1 of the photon with $J = 0$ of an even-even nucleus. Symmetry restoration techniques are also essential to obtain more realistic estimates of fission fragment characteristics, as was shown in the simplest case of particle number restoration [16,36]. Finally, correlation energies induced by symmetry restoration modify the overall PES, which could impact fission dynamics.

With the exception of several pioneering works [37–40], there has been no attempt at examining the impact of symmetry restoration in the context of fission. In addition to formal difficulties with symmetry restoration for standard functionals [25,41], the computational cost of probing a large number of extremely deformed configurations in heavy nuclei is prohibitively high, especially when simultaneously restoring multiple symmetries. In fact, symmetry-breaking PESs can usually only be computed by employing large harmonic oscillator (HO) bases with many incomplete shells which are not closed under spatial

rotations and for which conventional algorithms of rotational symmetry restoration are inapplicable [42].

In this Letter, we implement for the first time the technique of rotational symmetry restoration in incomplete bases originally proposed in Ref. [42], and perform the first symmetry restoration in ^{240}Pu from the ground state to scission. High-performance computing capabilities enable us to quantify the effect of particle number, angular momentum, and parity projections on the underlying PES and on the fission fragment mass distributions.

Method.—Symmetry-restored DFT is a two-step method. In the first step, we generated a set of axially symmetric HFB configurations with the HFBTHO package [43], using the SkM* parameterization of the Skyrme energy functional [44], a mixed volume-surface contact pairing force [45], and constraints on the values of the quadrupole (q_{20}) and octupole (q_{30}) moments. These quantities correspond to the elongation and the mass asymmetry of a nuclear shape, respectively, and arguably represent the most pertinent collective degrees of freedom for describing the fission phenomenon. The HFB equations were solved by expanding the solution in a deformed HO basis of $N_{\max} = 31$ incomplete shells with the corresponding lowest $N_{\mathrm{osc}} = 1100$ oscillator states included. The oscillator frequency and the basis deformation parameter were optimized for each $q \equiv (q_{20}, q_{30})$ configuration separately; more details on technical aspects of the HFB calculation can be found in Ref. [30].

In the next step, collective correlations related to the restoration of symmetries were incorporated by projecting the HFB configurations onto good values of angular momenta J, particle numbers (N, Z), and parity π. The projected kernels $\mathcal{K}_q^{J^\pi NZ}$ play the central role in this procedure,

$$\mathcal{K}_q^{J^\pi NZ} = \int_\beta \sum_{\varphi_n, \varphi_p} \mathcal{K}_q^{\beta, \varphi_n, \varphi_p}, \qquad (1)$$

where $\int_\beta \equiv (J + 1/2) \int_0^\pi d\beta \sin\beta d_{00}^{J*}(\beta)$ denotes integration over the rotational angle β with small Wigner matrices $d_{00}^{J*}(\beta)$ as weights, while $\sum_{\varphi_n, \varphi_p} \equiv \sum_{l_n, l_p=1}^{N_\varphi} e^{-iN_0\varphi_{l_n}} e^{-iZ_0\varphi_{l_p}}$ denotes Fomenko sums [46] over gauge angles $\varphi_{l_\tau} = l_\tau(\pi/N_\varphi)$ $(l_\tau = 0, \ldots, N_\varphi - 1)$ for neutrons $(\tau = n)$ and protons $(\tau = p)$. In our study, the projected kernel actually corresponds to the expectation value of the operator $\hat{O}$ in the symmetry-restored state. Therefore, the integrand of Eq. (1) can be written as

$$\mathcal{K}_q^{\mathbf{x}} = \langle \Phi(q) | \hat{O} e^{-i\beta \hat{J}_y} e^{i\varphi_n \hat{N}} e^{i\varphi_p \hat{Z}} \hat{P}^\pi | \Phi(q) \rangle, \qquad (2)$$

where we introduced $\mathbf{x} \equiv \{\beta, \varphi_n, \varphi_p\}$ for compactness, $e^{-i\beta \hat{J}_y} e^{i\varphi_n \hat{N}} e^{i\varphi_p \hat{Z}} \equiv \hat{R}$ is the rotation operator, $\hat{P}^\pi$ is the parity projection operator, and $\hat{J}_y$, $\hat{N}$, and $\hat{Z}$ correspond to

the y component of the total angular momentum, the neutron number, and the proton number operators, respectively. The norm overlap kernel $\mathcal{N}_q^{J^\pi NZ}$ is obtained by using Eqs. (1) and (2) with the identity operator, $\hat{O} = \hat{1}$, and the Hamiltonian kernel $\mathcal{H}_q^{J^\pi NZ}$ by using them with the nuclear Hamiltonian $\hat{H}$.

When computing large-scale PESs, it is customary to improve convergence by truncating and adjusting at each point q the characteristics of the underlying HO basis. However, the resulting basis is not closed under spatial rotations. Formally, given the rotational symmetry transformation $\mathcal{T}$ and a single-particle basis defined by the creation and annihilation operators $\{c_l^\dagger, c_k\}$, the rotated basis $\mathcal{T}^{-1}\{c_l^\dagger, c_k\}\mathcal{T}$ will contain states that are not present in the original basis. This prevents us from using conventional symmetry-restoring algorithms, which all assume closure of the basis under rotations. The elegant solution to this hurdle was proposed 25 years ago by Robledo [42], who reformulated the Wick theorem [47,48] to encompass bases not closed under symmetry transformations. Based on the formalism of Ref. [42], we can write the rotated norm overlap as

$$\mathcal{N}_q^{\mathbf{x}} = \sqrt{\det A_q^{\mathbf{x}} \times \det R^{\mathbf{x}}}, \qquad (3)$$

where

$$A_q^{\mathbf{x}} = U_q^T (R^{\mathbf{x}T})^{-1} U_q^* + V_q^T R^{\mathbf{x}} V_q^*. \qquad (4)$$

Here, U_q and V_q are the Bogoliubov matrices corresponding to the HFB configuration $|\Phi(q)\rangle$, and $R^{\mathbf{x}}$ denotes the matrix of the rotation operator $\hat{R}$ in the HO basis [49]. Note that in the case of a basis closed under rotations $|\det R^{\mathbf{x}}| = 1$, and the expression Eq. (3) reduces to the conventional Onishi formula [50]. In the symmetry-restored DFT framework, the Hamiltonian kernel $\mathcal{H}_q^{J^\pi NZ}$ is a functional of the one-body, transition density $\rho_q^{\mathbf{x}}$ and pairing tensor $\kappa_q^{\mathbf{x}}$. When the basis is not closed under rotations, these read

$$\rho_q^{\mathbf{x}} = R^{\mathbf{x}} V_q^* A_q^{\mathbf{x}-1} V_q^T, \qquad (5a)$$

$$\kappa_q^{\mathbf{x}} = R^{\mathbf{x}} V_q^* A_q^{\mathbf{x}-1} U_q^T, \qquad (5b)$$

where the mixed-density prescription was used [51]. The symmetry-restored energy is simply the ratio $\mathcal{E}_q^{J^\pi NZ} = \mathcal{H}_q^{J^\pi NZ} / \mathcal{N}_q^{J^\pi NZ}$.

Least-energy fission pathway.—Although distinct from the most probable fission path [52,53], the least-energy fission pathway provides valuable information about fission dynamics such as the existence and energies of fission barrier heights or fission isomers. These pseudodata are important to predict the stability of superheavy elements or
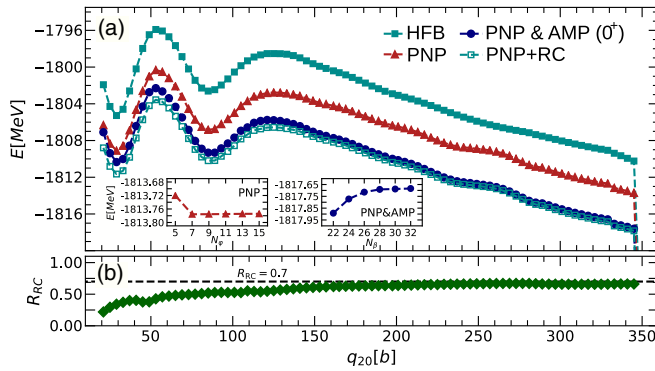
FIG. 1. (a) Least-energy fission pathway in ^{240}Pu calculated in the HFB approximation (turquoise squares); projected onto good values of particle numbers (PNP, red triangles); projected onto good values of particle numbers, angular momentum ($J = 0$) and parity (PNP & AMP, blue circles); obtained by adding the rotational correction E_{RC} on top of the PNP values (PNP + RC, empty squares). The insets show the convergence of the PNP and PNP & AMP for the pre-scission configuration with respect to the number of gauge angles N_φ and the number of rotational angles N_β, respectively. (b) Ratio $R_{RC} = (E_{PNP}^{0^+} - E_{PNP})/E_{PY}$; see text for details.

evaluate neutron-induced fission cross sections, especially in regions of the nuclide chart where no experimental data is available [54,55]. The goal of the present analysis is to assess the effect of symmetry restoration on such data along the entire fission pathway. In this regard, it represents an extension of the early work by Bender and co-workers who studied the effect of symmetry restoration along the reflection-symmetric ($q_{30} = 0$) pathway and up to moderate deformations only [37].

In the upper panel of Fig. 1 we plot the deformation energy of ^{240}Pu along the least-energy fission pathway as calculated in the HFB approximation (turquoise squares). Ninety-five configurations along the pathway were determined by constraining quadrupole moments within a range $21 \leq q_{20} \leq 397$ (in b) with steps $\Delta q_{20} = 4\,b$, while q_{30} moments were left unconstrained and determined self-consistently. We then projected these configurations onto good values of particle numbers (PNP, red triangles) and onto good values of particle numbers, angular momentum ($J = 0$), and parity (PNP & AMP, blue circles). The two insets in the upper panel of Fig. 1 show the convergence of the PNP and PNP & AMP procedures with respect to the number of integration points for the pre-scission configuration, $(q_{20}, q_{30}) = (345.0\,b, 42.6\,b^{3/2})$, where the underlying basis is the most incomplete. In order to ensure proper numerical convergence across all considered configurations, we set $N_\varphi = 9$ and $26 \leq N_\beta \leq 30$.

The potential energy curve of ^{240}Pu is characterized by two minima, the ground state and a fission isomer, and two fission barriers [56]. The scission point is marked by a sharp drop in energy, which occurs here at $q_{20} \approx 345\,b$. Table I lists the corresponding energies of these

TABLE I. Calculated excitation energies of the inner barrier, fission isomer, and outer barrier configuration, as well as the pre-scission energy (in MeV) along the HFB least-energy pathway, obtained with HFB, PNP, and PNP & AMP models.

Configuration	HFB	PNP	PNP & AMP
Inner barrier	9.37	8.78	8.05
Fission isomer	2.67	2.27	1.02
Outer barrier	6.75	6.28	4.58
Pre-scission	11.68	10.88	11.85

configurations. Although the HFB energy of the inner barrier (9.37 MeV) is about 3.3 MeV higher than the empirical value inferred from fission cross sections [57,58], this is mostly caused by the omission of triaxial effects in our calculations [59,60]: including them lowers the height of the first barrier by about 1.7 MeV [30]. This effect is amplified by symmetry restoration, which lowers the barrier by an additional 1.3 MeV, pushing the theoretical value well within the uncertainty limits of the empirical value (typically about 1 MeV). The outer barrier is axially symmetric and reflection asymmetric [30]. Its height is lowered by as much as 2.3 MeV by the symmetry restoration, again pushing the theoretical value within the 1 MeV limit of the empirical value, 5.15 MeV [58]. On the other hand, the HFB energy of the fission isomer is already in decent agreement with the empirical value of 2.25 ± 0.20 MeV [61]: symmetry restoration degrades this agreement. These numbers are consistent with those reported in Ref. [37].

While previous work in Refs. [37,38] was exclusively focused on the potential energy curve near the two barriers, we extend this study all the way to the scission point. Of particular interest is the pre-scission energy, which is defined as the energy difference between the outer barrier and the scission configuration, and which may provide an important contribution to the excitation energy of fission fragments. Interestingly, even though the corrections to the barriers are significant, we find that the total correlation energy beyond the outer barrier saturates, with the result that symmetry restoration has a negligible impact on the value of pre-scission energy.

In many studies of spontaneous fission, the effect of AMP is simulated by what is known as the rotational energy correction [10,62]. It was observed in Ref. [63] that this term is well approximated by $E_{RC} = 0.7 \times E_{PY}$ where $E_{PY} = -\langle \mathbf{J}^2 \rangle / (2\mathcal{J}_{PY})$, $\langle \mathbf{J}^2 \rangle$ is the total angular momentum dispersion, $\mathcal{J}_{PY}$ is the Peierls-Yoccoz moment of inertia [64], and the phenomenological quenching factor 0.7 is included to account for approximations introduced in calculating $\mathcal{J}_{PY}$. In panel (a) of Fig. 1 we also show the curve obtained by adding E_{RC} on top of the calculated PNP values (PNP + RC), while the ratio $R_{RC} = (E_{PNP}^{0^+} - E_{PNP})/E_{PY}$ is shown in the lower panel of Fig. 1. Our calculations confirm that E_{RC} is an excellent approximation
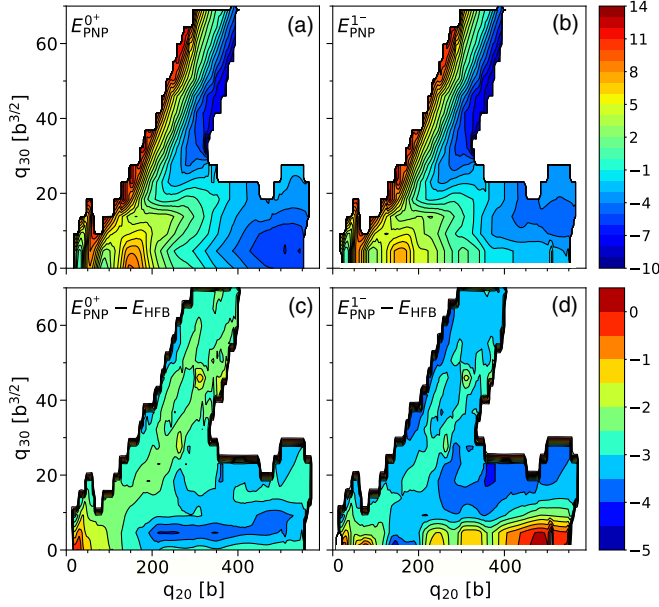
FIG. 2. (a) Two-dimensional symmetry-restored PES of ^{240}Pu in the (q_{20}, q_{30}) plane for the $J^{\pi} = 0^+$ configuration. (b) Same for $J^{\pi} = 1^-$. Both surfaces are normalized with respect to the energy of their respective ground states. (c) Difference between the symmetry-restored and the HFB surface for the $J^{\pi} = 0^+$ configuration. (d) Same for the $J^{\pi} = 1^-$.

FIG. 3. Primary fission fragment mass distributions in ^{240}Pu obtained from FELIX with the PES at the HFB level (blue squares) or after PNP & AMP for the 0^+ (orange circles) or 1^- (green triangles) states.

to the exact model at very large deformation and all the way to the scission point. However, we also observe that for configurations with $q_{20} \lesssim 150\,b$ the quenching factor of 0.7 is not sufficient, leading to differences in energy up to 2.5 MeV. This discrepancy could have a severe impact on observables that are very sensitive to details of the underlying PES, such as the spontaneous fission half-lives [11,31].

2D PES and fission fragment distributions.—While 1D fission paths can be sufficient to compute observables such as half-lives and cross sections, quantities such as fission fragment distributions require probing at least two dimensions in the collective space. Starting from the PES of ^{240}Pu in the HFB approximation reported in Ref. [30], we thus selected a total of 1150 configurations within 20 MeV of the ground state energy. They cover a very broad range of quadrupole and octupole deformations, with $20 \leq q_{20} \leq 567$ (in b) and $0 \leq q_{30} \leq 70$ (in $b^{3/2}$). We then projected each of these configurations onto good values of particle numbers, angular momentum, and parity using the above method [65].

Figure 2 shows the PES for the $J^{\pi} = 0^+$ (a) and $J^{\pi} = 1^-$ (b) states with the exact number of particles $N = 146$ and $Z = 94$. Although projection on 1^- is not possible for $q_{30} = 0\ \mathrm{b}^{3/2}$ configurations (indicated by a white line on the surface), we emphasize that the energy remains well defined and finite in the $q_{30} \rightarrow 0$ limit [66]. Overall, the PES retains its main features such as the fission isomer and the main fission valley, which extends from $(q_{20}, q_{30}) \approx (90\,b, 0\,b^{3/2})$ to $(q_{20}, q_{30}) \approx (340\,b, 40\,b^{3/2})$. Panels (c)

and (d), which show the energy difference between the symmetry-restored and HFB surfaces, provide an additional insight. In particular, for the 0^+ state, a pronounced gain in energy is observed at low q_{30} values for a wide range of configurations, pointing to the possible enhancement of symmetric fission. For the 1^- state, the correlation energy is large along and around the least-energy pathway, suggesting broader fission fragment distributions.

To estimate the actual effect on fission fragment distributions [65], we used the FELIX solver [67] to solve the collective Schrödinger equation originating from the Gaussian overlap approximation of the time-dependent GCM. The inputs to FELIX were the PESs (HFB and PNP & AMP for the 0^+ and 1^- states), the GCM inertia tensor computed at the perturbative cranking approximation, and scission configurations defined by the HFB expectation value of the Gaussian neck operator $q_N = 5$ with a folding factor of width $\sigma_A = 5$; see Ref. [13] for a discussion. To simulate the neutron-induced fission for thermal neutrons, the energy of the initial state was set at 1 MeV above the inner barrier. Figure 3 demonstrates the impact on the fragment mass distributions: fission becomes more symmetric after projections, and the symmetric fission mode is indeed enhanced for the 0^+ state. Furthermore, the distribution for the 1^- state is significantly broadened and favors less asymmetric fragmentations. Note that yields stemming from $q_{30} = 0\ b^{3/2}$ and nearby configurations are cautiously excluded from the plot (indicated by a gap in the curve). These results represent the first attempt to quantify the effect of symmetry restoration on actual fission observables. A fully consistent determination of fission fragment distributions will require developing a projected theory of collective inertia, estimating the spin distribution of the fissioning nucleus, and generating PESs with a much higher resolution in (q_{20}, q_{30}).

Conclusion.—Restoring broken symmetries is a necessary step for nuclear models to describe different fission channels. In this work, we reported the first symmetry-restoring description of fission from the ground state to scission. Our analysis of the benchmark case of ^{240}Pu indicates that projection correlation energies cannot be approximated by a phenomenological formula across the entire range of deformations relevant for fission, and that symmetry restoration may have a substantial impact on the mass distribution of fission fragments. These conclusions should be validated by developing a projected theory of collective inertia. The technique of symmetry restoration in incomplete bases is extendable to configuration mixing schemes, and could therefore be key to providing a reliable and computationally feasible framework for nuclear structure studies relevant to ongoing experimental programs at radioactive beam facilities.

[1] J. Beun, G. C. McLaughlin, R. Surman, and W. R. Hix, Fission cycling in a supernova r-process, Phys. Rev. C **77,** 035804 (2008).

[2] M. R. Mumpower, R. Surman, G. C. McLaughlin, and A. Aprahamian, The impact of individual nuclear properties on r-process nucleosynthesis, Prog. Part. Nucl. Phys. **86,** 86 (2016).

[3] M. R. Mumpower, T. Kawano, T. M. Sprouse, N. Vassh, E. M. Holmbeck, R. Surman, and P. Möller, β-delayed fission in r-process nucleosynthesis, Astrophys. J. **869,** 14 (2018).

[4] M. R. Mumpower, P. Jaffke, M. Verriere, and J. Randrup, Primary fission fragment mass yields across the chart of nuclides, Phys. Rev. C **101,** 054607 (2020).

[5] N. Vassh, R. Vogt, R. Surman, J. Randrup, T. M. Sprouse, M. R. Mumpower, P. Jaffke, D. Shaw, E. M. Holmbeck, Y. Zhu, and G. C. McLaughlin, Using excitation-energy dependent fission yields to identify key fissioning nuclei in r-process nucleosynthesis, J. Phys. G **46,** 065202 (2019).

[6] A. C. Hayes, Applications of nuclear physics, Rep. Prog. Phys. **80,** 026301 (2017).

[7] A. N. Andreyev, K. Nishio, and K.-H. Schmidt, Nuclear fission: A review of experimental advances and phenomenology, Rep. Prog. Phys. **81,** 016301 (2018).

[8] K.-H. Schmidt and B. Jurado, Review on the progress in nuclear fission—Experimental methods and theoretical descriptions, Rep. Prog. Phys. **81,** 106301 (2018).

[9] H. J. Krappe and K. Pomorski, *Theory of Nuclear Fission* (Springer, New York, 2012).

[10] N. Schunck and L. M. Robledo, Microscopic theory of nuclear fission: A review, Rep. Prog. Phys. **79,** 116301 (2016).

[11] A. Baran, M. Kowal, P.-G. Reinhard, L. M. Robledo, A. Staszczak, and M. Warda, Fission barriers and probabilities of spontaneous fission for elements with $Z \geq 100$, Nucl. Phys. **A944,** 442 (2015).

[12] H. Goutte, P. Casoli, and J.-F. Berger, Mass and kinetic energy distributions of fission fragments using the time dependent generator coordinate method, Nucl. Phys. **A734,** 217 (2004).

[13] D. Regnier, N. Dubray, N. Schunck, and M. Verrière, Fission fragment charge and mass distributions in ^{239}Pu(n, f) in the adiabatic nuclear energy density functional theory, Phys. Rev. C **93,** 054611 (2016).

[14] H. Tao, J. Zhao, Z. P. Li, T. Nikšić, and D. Vretenar, Microscopic study of induced fission dynamics of ^{226}Th with covariant energy density functionals, Phys. Rev. C **96,** 024319 (2017).

[15] D. Regnier, N. Dubray, and N. Schunck, From asymmetric to symmetric fission in the Fermium isotopes within the time-dependent generator-coordinate-method formalism, Phys. Rev. C **99,** 024611 (2019).

[16] M. Verrière, N. Schunck, and T. Kawano, Number of particles in fission fragments, Phys. Rev. C **100,** 024612 (2019).

[17] J. Zhao, T. Nikšić, D. Vretenar, and S.-G. Zhou, Microscopic self-consistent description of induced fission dynamics: Finite-temperature effects, Phys. Rev. C **99,** 014618 (2019).

[18] J. Zhao, J. Xiang, Z.-P. Li, T. Nikšić, D. Vretenar, and S.-G. Zhou, Time-dependent generator-coordinate-method study of mass-asymmetric fission of actinides, Phys. Rev. C **99,** 054613 (2019).

[19] C. Simenel and A. S. Umar, Formation and dynamics of fission fragments, Phys. Rev. C **89,** 031601(R) (2014).

[20] A. Bulgac, P. Magierski, K. J. Roche, and I. Stetcu, Induced Fission of ^{240}Pu within a Real-Time Microscopic Framework, Phys. Rev. Lett. **116,** 122504 (2016).

[21] A. Bulgac, S. Jin, K. J. Roche, N. Schunck, and I. Stetcu, Fission dynamics of ^{240}Pu from saddle to scission and beyond, Phys. Rev. C **100,** 034615 (2019).

[22] N. Bohr and J. A. Wheeler, The mechanism of nuclear fission, Phys. Rev. **56,** 426 (1939).

[23] A. Klein, N. R. Walet, and G. D. Dang, Classical theory of collective motion in the large amplitude, small velocity regime, Ann. Phys. (N.Y.) **208,** 90 (1991).

[24] N. Schunck, *Energy Density Functional Methods for Atomic Nuclei*, IOP Expanding Physics (IOP Publishing, Bristol, UK, 2019).

[25] J. A. Sheikh, J. Dobaczewski, P. Ring, L. M. Robledo, and C. Yannouleas, Symmetry restoration in mean-field approaches, arXiv:1901.06992.

[26] *Nuclear Superfluidity—Pairing in Finite Systems*, edited by D. M. Brink and R. A. Broglia (Cambridge University Press, Cambridge, England, 2005).

[27] P.-G. Reinhard and K. Goeke, The generator coordinate method and quantised collective motion in nuclear systems, Rep. Prog. Phys. **50,** 1 (1987).

[28] J. F. Berger, M. Girod, and D. Gogny, Time-dependent quantum collective dynamics applied to nuclear fission, Comput. Phys. Commun. 63, 365 (1991).

[29] A. Staszczak, A. Baran, J. Dobaczewski, and W. Nazarewicz, Microscopic description of complex nuclear decay: Multimodal fission, Phys. Rev. C 80, 014309 (2009).

[30] N. Schunck, D. Duke, H. Carr, and A. Knoll, Description of induced nuclear fission with Skyrme energy functionals: Static potential energy surfaces and fission fragment properties, Phys. Rev. C 90, 054305 (2014).

[31] M. Warda and J. L. Egido, Fission half-lives of superheavy nuclei in a microscopic approach, Phys. Rev. C 86, 014322 (2012).

[32] R. Rodríguez-Guzmán and L. M. Robledo, Microscopic description of fission in uranium isotopes with the Gogny energy density functional, Phys. Rev. C 89, 054310 (2014).

[33] B.-N. Lu, E.-G. Zhao, and S.-G. Zhou, Potential energy surfaces of actinide nuclei from a multidimensional constrained covariant density functional theory: Barrier heights and saddle point shapes, Phys. Rev. C 85, 011301 (2012).

[34] J. Zhao, B.-N. Lu, D. Vretenar, E.-G. Zhao, and S.-G. Zhou, Multidimensionally constrained relativistic mean-field study of triple-humped barriers in actinides, Phys. Rev. C 91, 014321 (2015).

[35] Krishichayan, M. Bhike, C. R. Howell, A. P. Tonchev, and W. Tornow, Fission product yield measurements using monoenergetic photon beams, Phys. Rev. C 100, 014608 (2019).

[36] G. Scamps and Y. Hashimoto, Transfer probabilities for the reactions ^{14,20}O $+^{20}$O in terms of multiple time-dependent Hartree-Fock-Bogoliubov trajectories, Phys. Rev. C 96, 031602 (2017).

[37] M. Bender, P.-H. Heenen, and P. Bonche, Microscopic study of ^{240}Pu: Mean field and beyond, Phys. Rev. C 70, 054304 (2004).

[38] M. Samyn, S. Goriely, and J. Pearson, Further explorations of Skyrme-Hartree-Fock-Bogoliubov mass formulas. V. Extension to fission barriers, Phys. Rev. C 72, 044316 (2005).

[39] T. V. N. Hao, P. Quentin, and L. Bonneau, Parity restoration in the highly truncated diagonalization approach: Application to the outer fission barrier of ^{240}Pu, Phys. Rev. C 86, 064307 (2012).

[40] R. Bernard, S. A. Giuliani, and L. M. Robledo, Role of dynamic pairing correlations in fission dynamics, Phys. Rev. C 99, 064301 (2019).

[41] T. Duguet, M. Bender, K. Bennaceur, D. Lacroix, and T. Lesinski, Particle-number restoration within the energy density functional formalism: Nonviability of terms depending on noninteger powers of the density matrices, Phys. Rev. C 79, 044320 (2009).

[42] L. M. Robledo, Practical formulation of the extended Wick's theorem and the Onishi formula, Phys. Rev. C 50, 2874 (1994).

[43] R. N. Perez, N. Schunck, R.-D. Lasseri, C. Zhang, and J. Sarich, Axially deformed solution of the Skyrme–Hartree–Fock–Bogolyubov equations using the transformed harmonic oscillator basis (III) HFBTHO (v3.00): A new version of the program, Comput. Phys. Commun. 220, 363 (2017).

[44] J. Bartel, P. Quentin, M. Brack, C. Guet, and H.-B. Håkansson, Towards a better parametrisation of Skyrme-like effective forces: A critical study of the SkM force, Nucl. Phys. A386, 79 (1982).

[45] J. Dobaczewski, W. Nazarewicz, and M. V. Stoitsov, Contact pairing interaction for the Hartree-Fock-Bogoliubov calculations, in The Nuclear Many-Body Problem 2001, Nato Science Series II Vol. 53 (Springer, Netherlands, 2002), P. 181.

[46] V. N. Fomenko, Projection in the occupation-number space and the canonical transformation, J. Phys. A 3, 8 (1970).

[47] R. Balian and E. Brezin, Nonunitary Bogoliubov transformations and extension of Wick's theorem, Nuovo Cimento B 64, 37 (1969).

[48] K. Hara and S. Iwasaki, On the quantum number projection, Nucl. Phys. A332, 61 (1979).

[49] R. G. Nazmitdinov, L. M. Robledo, P. Ring, and J. L. Egido, Representation of three-dimensional rotations in oscillator basis sets, Nucl. Phys. A596, 53 (1996).

[50] N. Onishi and S. Yoshida, Generator coordinate method applied to nuclei in the transition region, Nucl. Phys. 80, 367 (1966).

[51] L. M. Robledo, Remarks on the use of projected densities in the density-dependent part of Skyrme or Gogny functionals, J. Phys. G 37, 064020 (2010).

[52] J. Sadhukhan, K. Mazurek, A. Baran, J. Dobaczewski, W. Nazarewicz, and J. A. Sheikh, Spontaneous fission lifetimes from the minimization of self-consistent collective action, Phys. Rev. C 88, 064314 (2013).

[53] S. A. Giuliani and L. M. Robledo, Fission properties of the Barcelona-Catania-Paris-Madrid energy density functional, Phys. Rev. C 88, 054325 (2013).

[54] M. Sin, R. Capote, A. Ventura, M. Herman, and P. Obložinský, Fission of light actinides: Th232(n,f) and Pa231(n,f) reactions, Phys. Rev. C 74, 014608 (2006).

[55] S. Goriely, S. Hilaire, A. J. Koning, M. Sin, and R. Capote, Towards a prediction of fission cross sections on the basis of microscopic nuclear inputs, Phys. Rev. C 79, 024612 (2009).

[56] S. Bjørnholm and J. E. Lynn, The double-humped fission barrier, Rev. Mod. Phys. 52, 725 (1980).

[57] G. N. Smirenkin, Preparation of evaluated data for a fission barrier parameter library for isotopes with $Z = 82$–98, with consideration of the level density models used, International Atomic Energy Agency (IAEA) Technical Report No. INDC(CCP)-359, 1993.

[58] R. Capote et al., RIPL–Reference input parameter library for calculation of nuclear reactions and nuclear data evaluations, Nucl. Data Sheets 110, 3107 (2009).

[59] S. E. Larsson, I. Ragnarsson, and S. G. Nilsson, Fission barriers and the inclusion of axial asymmetry, Phys. Lett. 38B, 269 (1972).

[60] M. Girod and B. Grammaticos, Triaxial Hartree-Fock-Bogolyubov calculations with D1 effective interaction, Phys. Rev. C 27, 2317 (1983).

[61] M. Hunyadi, D. Gassmann, A. Krasznahorkay, D. Habs, P. G. Thirolf, M. Csatlós, Y. Eisermann, T. Faestermann, G. Graw, J. Gulyás, R. Hertenberger, H. J. Maier, Z. Máté, A. Metz, and M. J. Chromik, Excited superdeformed $K^{\pi} = 0^{+}$ rotational bands in β-vibrational fission resonances of ^{240}Pu, Phys. Lett. B 505, 27 (2001).

[62] J. L. Egido and L. M. Robledo, 10 Angular momentum projection and quadrupole correlations effects in atomic nuclei, in *Extended Density Functionals in Nuclear Structure Physics*, edited by G. A. Lalazissis, P. Ring, and D. Vretenar, Lecture Notes in Physics Vol. 641 (Springer, Berlin, Heidelberg, 2004), https://link.springer.com/chapter/10.1007%2F978-3-540-39911-7_10.

[63] J. L. Egido and L. M. Robledo, Fission Barriers at High Angular Momentum and the Ground State Rotational Band of the Nucleus ^{254}No, Phys. Rev. Lett. **85**, 1198 (2000).

[64] R. E. Peierls and J. Yoccoz, The collective model of nuclear motion, Proc. Phys. Soc. London Sect. A **70**, 381 (1957).

[65] See Supplemental Material at http://link.aps.org/supplemental/10.1103/PhysRevLett.125.102504 for a discussion on convergence of the PNP procedure and for more details on validity of using the TDGCM + GOA framework with symmetry-restored potential energy surfaces.

[66] J. L. Egido and L. M. Robledo, Parity-projected calculations on octupole deformed nuclei, Nucl. Phys. **A524**, 65 (1991).

[67] D. Regnier, N. Dubray, M. Verrière, and N. Schunck, FELIX-2.0: New version of the finite element solver for the time dependent generator coordinate method with the Gaussian overlap approximation, Comput. Phys. Commun. **225**, 180 (2018).